SCIENTIFIC REP♦RTS

OPEN

Far-Infrared and Raman Spectroscopy Investigation of Phonon Modes in Amorphous and Crystalline Epitaxial GeTe-Sb$_2$Te$_3$ Alloys

V. Bragaglia[1], K. Holldack[2], J. E. Boschker[1], F. Arciprete[1,3], E. Zallo[1], T. Flissikowski[1] & R. Calarco[1]

A combination of far-infrared and Raman spectroscopy is employed to investigate vibrational modes and the carrier behavior in amorphous and crystalline ordered GeTe-Sb$_2$Te$_3$ alloys (GST) epitaxially grown on Si(111). The infrared active GST mode is not observed in the Raman spectra and vice versa, indication of the fact that inversion symmetry is preserved in the metastable cubic phase in accordance with the F$\bar{3}$m3 space group. For the trigonal phase, instead, a partial symmetry break due to Ge/Sb mixed anion layers is observed. By studying the crystallization process upon annealing with both the techniques, we identify temperature regions corresponding to the occurrence of different phases as well as the transition from one phase to the next. Activation energies of 0.43 eV and 0.08 eV for the electron conduction are obtained for both cubic and trigonal phases, respectively. In addition a metal-insulator transition is clearly identified to occur at the onset of the transition between the disordered and the ordered cubic phase.

GeTe-Sb$_2$Te$_3$ alloys (GST) are highly interesting compounds in terms of both fundamental investigations on phase change properties and technological applications in memory devices[1,2]. In phase change memories devices, the metastable crystalline phase of GST is utilized as the memory SET state, whereas the RESET state is realized in the amorphous phase[1]. The dramatic differences in physical properties such as resistivity between the amorphous and crystalline phase of GST are primarily due to the change in the character of the chemical bonds from covalent in the amorphous to resonant in the crystalline phase[3]. In addition to the amorphous to crystalline transition, a metal-insulator-transition (MIT) is evidenced[4–6] within the metastable phase of GST (disordered cubic to ordered cubic). Both changes in bonding as well as in symmetry are perfectly suited to be investigated by Raman scattering as well as for far-infrared (FIR) spectroscopy. In addition, the included THz spectral range is particularly sensitive to conductivity changes depending on the phase. However, while Raman spectroscopy was often employed for such alloys[7–11], the latter technique was mostly applied to Sb$_2$Te$_3$[10], with the exception of dynamic experiments[12].

Recently, we were able to achieve a fundamental advance in the fabrication of GST by molecular beam epitaxy (MBE) resulting in as-deposited single-crystalline material with out-of-plane stacking of vacancy layers[6], a highly-ordered structure with both cubic and rhombohedral stacking. Most interestingly, highly-ordered cubic GST (c-GST) is also obtained-through annealing treatment of amorphous GST (a-GST) deposited on a crystalline substrate[6,13]. In this case, it is possible to slowly tune the structural transitions (amorphous to crystalline and cubic to trigonal) to identify both the change in bonding and symmetry.

In this study we performed a combination of FIR and Raman spectroscopy to investigate vibrational modes in amorphous and crystalline epitaxially grown as well as annealed GST samples. We assign the observed phonon modes to the different crystalline phases by comparing temperature dependent FIR and Raman spectra. By FIR

[1]Paul-Drude-Institut für Festkörperelektronik, Hausvogteiplatz 5-7, 10117 Berlin, Germany. [2]Helmholtz-Zentrum Berlin für Materialien und Energie GmbH, Albert-Einstein-Str. 15, D-12489, Berlin, Germany. [3]Dipartimento di Fisica, Università di Roma "Tor Vergata", Via della Ricerca Scientifica 1, I-00133 Rome, Italy. Correspondence and requests for materials should be addressed to R.C. (email: calarco@pdi-berlin.de)

1
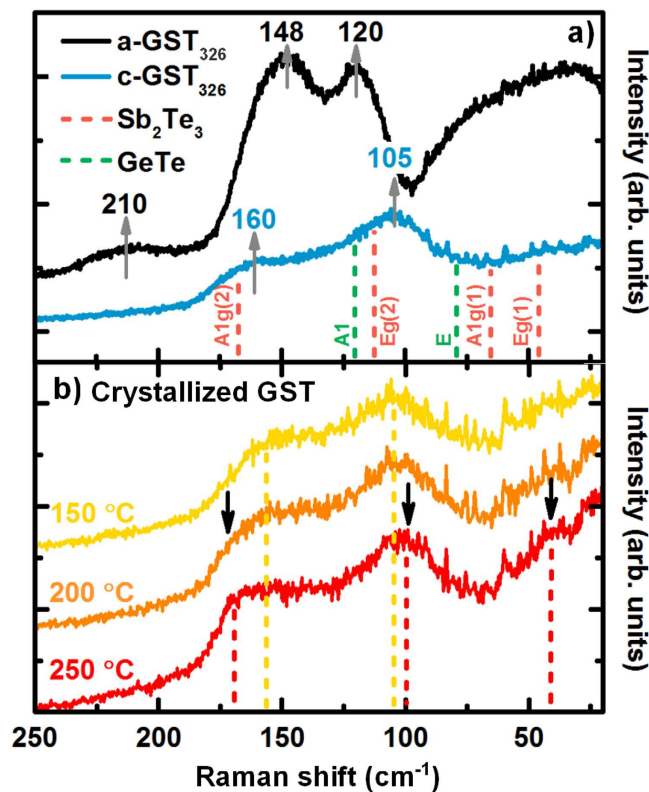
Figure 1. (**a**) Comparison of Raman spectra for a-GST326 (black) and as grown c-GST326 (blue); gray arrows highlight the mode positions. Sb_2Te_3 (red) and GeTe (green) Raman mode positions are plotted as references. (**b**) Raman spectra of crystallizing a-GST326 for three different temperatures. Modes of metastable c-GST326 are highlighted with yellow dashed lines. Upon increasing the temperature new modes appear, indication of the transition from c- to t-GST. At $T = 200\,^{\circ}C$ the characteristic mode of t-GST ($\sim 170\,cm^{-1}$) appears (red dashed lines). In the red curve ($T = 200\,^{\circ}C$) the two arrows highlight the other two modes of the t-GST.

absorption we discriminate between the contributions of phonons and free carrier delocalization upon sample annealing for both amorphous to crystalline and insulating to metal transitions.

Results and Discussion

In Fig. 1(a) Raman spectra of a- and c-GST326 samples are presented in the spectral range from $30\,cm^{-1}$ to $250\,cm^{-1}$. The a-GST spectrum presents the characteristic Bose peak (30–$100\,cm^{-1}$)[9], and two modes centered at 120 and $148\,cm^{-1}$, assigned to vibrations of defective octahedra[14]. The broad feature at $210\,cm^{-1}$ is ascribed to vibrations of tetrahedra[14]. In the c-GST spectrum two strong broad modes centered at 105 and $160\,cm^{-1}$ are present. Polarization dependent measurements (not shown) help to assign the modes to E_g ($105\,cm^{-1}$) and A_{1g} ($160\,cm^{-1}$). Such modes are characteristic of the metastable cubic c-GST phase (point group $m\bar{3}m$) in accordance with previous studies[14]. According to the $F\bar{3}m3$ space group expected for metastable c-GST, and the sites occupancy given from Nonaka *et al.*[15], no Raman active modes should be allowed, and only the T_{1u} (IR active mode, see later in the text) is expected. The fact that such vibrations (E_g and A_{1g}) are observed and are broad, is attributed to the presence of vacancies and defects that are responsible for the local symmetry breaking[14]. The fluctuation of compositions has been evidenced in a formerly published paper[6] and is intrinsic for certain GST compositions. Due to the broad nature of c-GST vibrational modes, the treatment of such fluctuation is not obvious. Both binary compounds constituting GST are measured for reference purposes and the peak position are displayed in Fig. 1(a) with green (α-GeTe - R3m space group) and red (Sb_2Te_3–$R\bar{3}m$ space group) dotted lines. The Raman modes of the metastable c-GST326 [Fig. 1(a) blue curve] are prevalently arising from the Sb_2Te_3 modes $A_{1g}(2)$ and $E_g(2)$ slightly shifted ($\sim 7\,cm^{-1}$) toward lower energies, while the modes of GeTe do not strongly contribute, due to their lower polarizability if compared to Sb_2Te_3, as already reported in literature[9,14] (see Table 1 for peak positions, mode assignments and their IR and Raman activities). In particular the mode at $160\,cm^{-1}$ has a one-mode behavior (Sb_2Te_3-like) while the mode at $105\,cm^{-1}$ has a two modes behavior (Sb_2Te_3-like and GeTe-like). The mode position shift of the c-GST326, compared to the binary constituents, is the indication of mode wavenumbers compositional dependence, similarly as for transition metal di-chalcogenides[16].

In order to study the temperature dependence of the vibrational modes, annealing of a-GST326 was performed *in-situ* during Raman data acquisition. A representative selection of the resulting spectra is plotted in Fig. 1(b). At $T = 150\,^{\circ}C$ (yellow curve) characteristic modes of the cubic phase (dotted yellow lines) compare well with those reported in Fig. 1(a) for the as grown c-GST326. At $T = 250\,^{\circ}C$ the film is transformed into the trigonal phase, t-GST (red curve), for which three modes are identified[17]: two evident at $170\,cm^{-1}$ (A) and $100\,cm^{-1}$ (E)

| Mode	(cm^{-1})	IR	Raman
a-GST			
A1	120	no	yes
A1	148	no	yes
	210	no	yes
c-GST			
T_{1u}	70	yes	no
E_g	105	no	yes
	120	yes	no
A_{1g}	160	no	yes
t-GST			
A-type	45	no	yes
E-type	100	yes	yes
A-type	170	no	yes
Sb$_2$Te$_3$			
$E_g(1)$	48	no	yes
$A_u(1)$	62	yes	no
$A_{1g}(1)$	67	no	yes
$E_g(2)$	113	no	yes
$A_{1g}(2)$	165	no	yes
GeTe			
E	79	yes	yes
A1	119	yes	yes

Table 1. Vibrational mode assignment and position for a-GST326, c-GST (both 225 and 326), t-GST, Sb$_2$Te$_3$ and GeTe. IR and Raman activity are specified. Note that the position of T_{1u} for c-GST is reported as the convolution of the two peaks at 60 cm^{-1} (GST225) and 80 cm^{-1} (GST326), according to Fig. 2. See text for details.

and a faint one at 45 cm^{-1} (A). The mode at 170 cm^{-1} starts to be visible in the spectra at T = 200 °C (see arrow on the orange curve), and could be associated to vacancies ordering into layers which breaks locally the cubic symmetry, and will transform into van der Waals gaps once the t-GST is achieved (red curve). The progressive creation of ordered vacancy layers obscures the unequivocal assignment of a specific space group within the transition region. As reported in our previous studies[13], we cannot exclude possible compositional rearrangement in the stable phase.

Figure 2(a) shows the FIR absorbance of MBE gorwn a-GST326 (black curve) and c-GST326 (blue curve) [Absorbance = −Log (T$_{GST}$/T$_{Si}$) where T$_{GST}$ and T$_{Si}$ are the GST and Si transmitted intensities]. Within the resolution of the measurement, no absorption in the whole spectral range is measured for a-GST326, in line with the absence of free carriers in the amorphous phase and due to a random distribution of local dipoles. On the contrary, c-GST326 shows a strong absorption on the whole spectral range which is an indication of metallic behavior with high free carrier concentration (~10^{20} cm^{-3} measured by low temperature transport measurement) and a broad (FWHM ~40 cm^{-1}) absorption feature around 70 cm^{-1}. In a-GST carriers are localized[3,5,18] while in c-GST delocalized electrons allows for the conduction[4,5]. For c-GST we divide the spectral range into two main regions: the phonon dominated region between 30 and 150 cm^{-1}, that we assume to be sensitive to the lattice transformations upon phase transitions, and the free carrier dominated region above 150 cm^{-1}.

Figure 2(b) shows a dedicated measurement with high resolution around the phonon related absorption feature for MBE grown c-GST326 (blue), GeTe (green) and Sb$_2$Te$_3$ (red). Sb$_2$Te$_3$ displays a peak at 62 cm^{-1}, which corresponds to the A_{1u} mode for the symmetry R$\bar{3}$m, while α-GeTe presents two peaks at 79 cm^{-1} and 119 cm^{-1} (grey dashed line in the plot), attributed to the E and A_{1u} modes, respectively (see also Raman spectrum). In the case of c-GST326, the IR phonon mode centered at ~70 cm^{-1}, according to the m$\bar{3}$m point group of the cubic symmetry, is attributed to a T_{1u}. However, as already mentioned, vacancies, defects and distortion of bonds could break the inversion symmetry predicted by the space group, leading to a mixed nature of the phonon modes[19]. The broad mode T_{1u} of c-GST326 is composed by the superposition of the phonon modes of the binary constituent compounds, E and A_{1u} for GeTe and Sb$_2$Te$_3$, respectively, [see Fig. 2(c,d)] since it is possible to best fit the peak with two Lorentzian functions centered at the experimental positions of the GeTe and Sb$_2$Te$_3$ modes, indicating a two-modes type behavior (Sb$_2$Te$_3$ and GeTe-like). As opposed to Raman spectroscopy, the two binary component modes show no wavenumber dependency on GST composition. The latter is accounted only in the relative intensities of the two modes. In particular the main contribution, comparing peak intensities, is the E mode of GeTe, for c-GST326 [see Fig. 2(c)] where more Ge-Te than Sb-Te bonds are expected. Instead, for the c-GST225 case [see Fig. 2(d)] a slightly higher intensity of the Sb$_2$Te$_3$ component is visible. FIR spectroscopy thus helps in the quantification of compositional changes.

Crystallization by annealing of a-GST326 was also studied by *in-situ* temperature dependent FIR spectroscopy. The phonon dominated region is shown in Fig. 3(a) where the absorption (Absorption = 1 − (T$_{GST}$ − T$_{Si}$)/T$_0$, with T$_0$ the incident intensity) increases with the annealing temperature from a value close to zero till a maximum
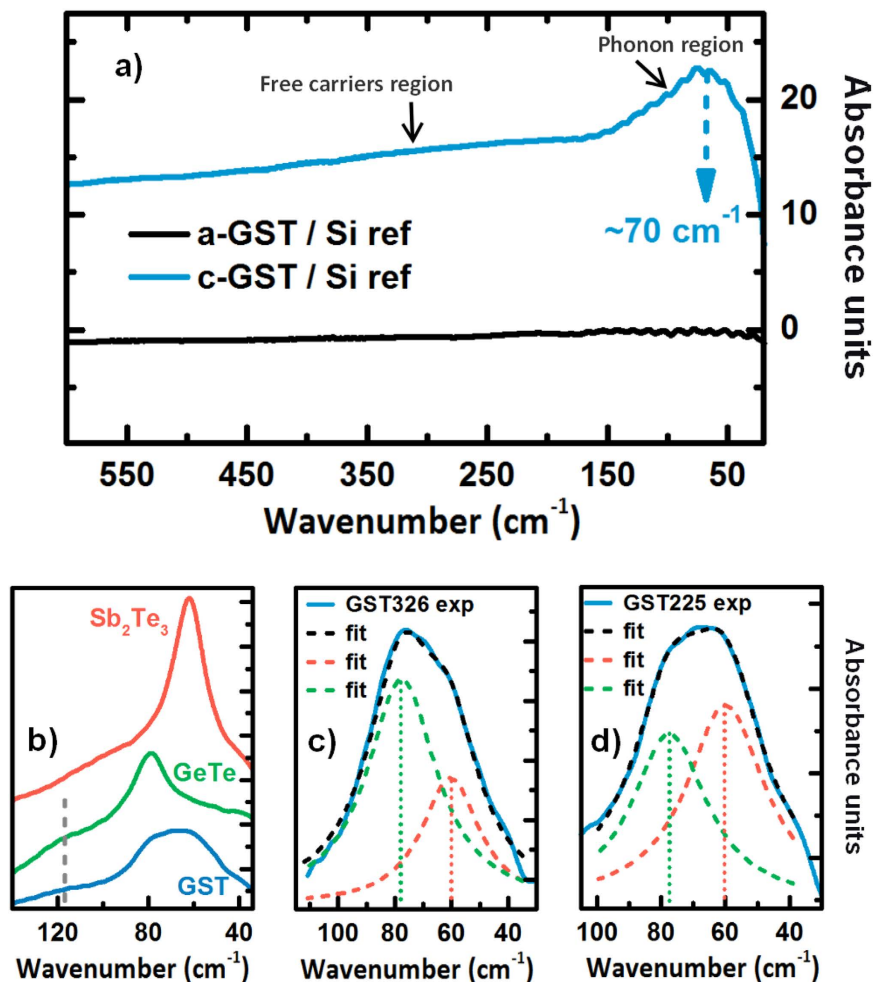
Figure 2. (**a**) FIR absorbance spectra for a-GST326 and c-GST326, black and blue curves, respectively. The spectra are normalized to the Si substrate. (**b**) Zoom around GST225 absorption feature (30 to 140 cm^{-1}) (blue), with Sb$_2$Te$_3$ (red) and GeTe (green) spectra as references. (**c**) Fit of the GST326 experimental curve using two Lorentzian peaks centered at the position of the Sb$_2$Te$_3$ (red) and GeTe (blue) modes. (**d**) Fit of GST225 for comparison.

value of 14%. Please note that at high resolution, a faint mode at 80 cm^{-1} is visible in a-GST326, indicative of the presence of short range ordering. In addition, starting at 206 °C the main peak at 80 cm^{-1} (P$_1$, see grey dotted line) attributed to c-GST326 decreases while a new mode at ~100 cm^{-1} ascribed to t-GST emerges (P$_2$ black arrow and grey dotted line in Fig. 3(a)). P$_2$ becomes more evident at higher annealing temperature [red curve Fig. 3(a)] when the film is completely trigonal (T > 225 °C), in accordance with Raman spectra in Fig. 1(b).

As-grown c-GST326 as well as a-GST326 crystallized at low annealing temperatures [T = 150 °C in Fig. 1(b)] belong to the m$\bar{3}$m point group with the exclusion (IR vs. Raman) selection rule preserved. Once the cubic to trigonal phase transition takes place, if we exclude a transition region where both modes characteristic of the two phases (P$_1$ at 80 cm^{-1} for the cubic and P$_2$ at 100 cm^{-1} for the trigonal) coexist and the symmetry determination is not possible, the exclusion selection rule seems not to hold and the mode at 100 cm^{-1} appears in both Raman (see Fig. 1(b)) and IR spectra (clearly evident in the completely t-GST annealed at 250 °C). According to literature, symmetry change between the two phases takes place from the m$\bar{3}$m to the expected $\bar{3}$m point group, with t-GST belonging to the space group R$\bar{3}$m or P$\bar{3}$m1 depending on the composition[20], for which mutual exclusion selection rules are valid. However, in Sosso *et al.*[17] the effect of mixed Ge/Sb layers is shown to induce a partial break of the symmetry, from P$\bar{3}$m1 to a lower symmetry state, where the Pm symmetry is preserved, allowing the double character (both Raman and IR) of the modes.

Several Arrhenius plots are extracted from the absorption spectra and plotted as a function of $1/k_BT$ in Fig. 3(b,c). The contribution arising from phonons (see Fig. 3(a)) is shown by circles, blue for P$_1$ (c-GST326) and red for P$_2$ (t-GST). Four main regions can be identified: white for a-GST, blue for the transition region from a-GST to c-GST, orange for the transition from c- to t-GST and red for t-GST. The annealing temperature ranges agree well with that of our previous XRD studies[6,13]. Please note that a full disordered c-GST326 is obtained at 130 °C[13] and it is ordered at about 183 °C[6], while t-GST is present already at 225 °C. From the slope of the curves in the linear blue region an activation energy for the conduction of c-GST326 is extracted, this giving
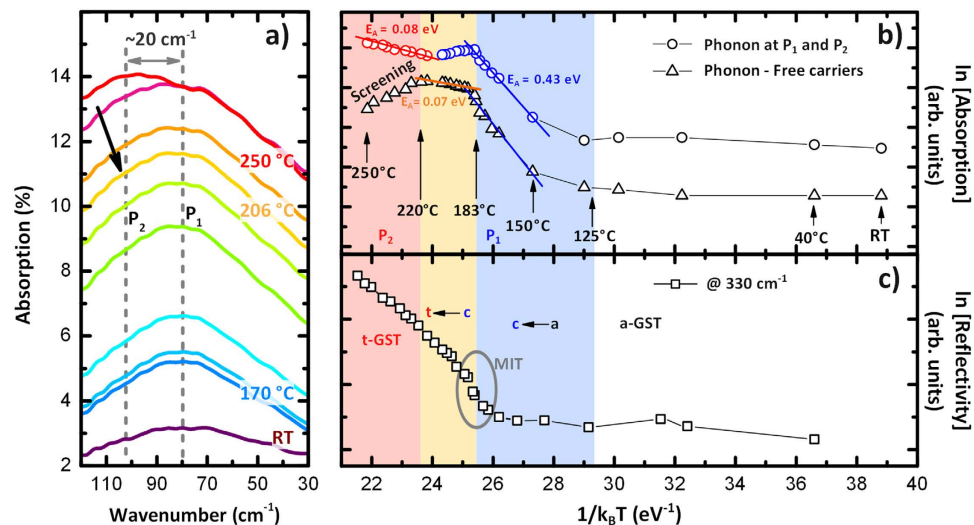
Figure 3. (**a**) Temperature dependent absorption spectra of crystallizing a-GST326 around the main absorption feature. (**b**) Arrhenius plot based on the intensity evolution of the phonon dominated region: peak P_1 for c-GST326 and P_2 for t-GST (empty circles), and difference between phonon and carrier dominated region (at $330\,cm^{-1}$) intensities evolution (empty triangles). Activation energy of the conduction process (blue for cubic- and red for t-GST) are obtained after fitting. (**c**) Arrhenius plot of the evolution of the reflectivity at $330\,cm^{-1}$. Four main regions are visible in (**b,c**): white for a-GST326, blue for c-GST326, orange for the transition from c- to t-GST and red for t-GST.

$E_A = 0.43\,eV$, a value which compares well with literature[21,22]. In the red region (t-GST) the slope of P_2 has an activation energy of $E_A = 0.08\,eV$, indication of an enhanced metallic behavior. Additional information can be obtained if we consider the difference (triangles in Fig. 3(b)) between the absorption of phonons (P_1 and P_2) and free carriers (at $330\,cm^{-1}$). For temperatures lower than 183 °C the P_1 phonon evolution, indication of a-GST326 to c-GST326 phase transformation, is dominant, as the two curves (circles and triangles) display the same shape. Above 220 °C, the free carriers are screening the P_2 phonon, suggesting longitudinal nature for P_2 in the trigonal phase. In the transition region between c- and t-GST the progressive ordering of vacancies into layers, till the formation of van der Waals gaps, leads to free carrier delocalization and metallic behavior with an activation energy $E_A = 0.07\,eV$ (orange line).

In Fig. 3(c) we display the Arrhenius plot of the reflectivity at $330\,cm^{-1}$. Although the absolute values could be not reliable as the measured sample is very thin (~30 nm), however, we clearly see that the reflectivity increases continuously during annealing induced transition from c-GST to t-GST, indication of the enhanced metallic behavior of the sample. The reflectivity increases significantly only at about T = 176 °C that we can identify as the temperature for the MIT to occur, as it corresponds to the sudden increase in conduction[6]. Above T = 183 °C a second trend can be identified, and is ascribed to the cubic to trigonal phase transition that proceeds gradually. Furthermore, the increase of reflectivity above 220 °C reflects the increase of free carrier delocalization and confirms their dominant role in screening the phonon.

In conclusions within this study we assign the symmetries to the crystalline phases of GST326 by comparing FIR and Raman temperature dependent spectra. Ordered c-GST is ascribed to the $F\bar{3}m3$ space group, while as for t-GST the inversion selection rules do not hold, a partial symmetry breaking due to Ge/Sb mixed anion layers[17] occurs. We have also demonstrated that FIR spectroscopy is sensitive to composition difference in as grown crystalline GST samples and helps in quantification of conduction enhancement/carrier behavior upon phase transitions. Furthermore, by studying the FIR absorption evolution upon annealing, we discriminate the contributions of phonons, and free carrier delocalization for the conduction of c-GST326 and t-GST, as well as for the transition regions a-GST326 to c-GST326 and c- to t-GST. In addition, from the reflectivity change the MIT is clearly identified and occurs at the onset between disordered to ordered cubic phase, in line with our previous results[6].

Methods

MBE growth. A series of Sb_2Te_3[23], GeTe[24,25], a-GST and metastable c-GST films with compositions Ge : 3 Sb : 2 Te : 6 (326) and Ge : 2 Sb : 2 Te : 5 (225), unintentionally doped, were deposited by MBE[23] on a highly resistive (5 kΩcm^{-1}) crystalline Si(111)-($\sqrt{3} \times \sqrt{3}$)R30°-Sb surface[23] with a thickness ranging between 30 and 40 nm. The samples were capped with 30 nm of Si_3N_4 by sputtering to prevent oxidation of the films.

XRD. Samples were characterized by means of *ex-situ* X-ray diffraction (XRD), utilizing a PANalytical X' Pert PRO MRD diffractometer with Ge (220) hybrid monochromator, employing a Cu Kα$_1$ radiation (λ = 1.540598 Å). XRD revealed that the crystalline GST films are quasi single crystalline[13,26] with vacancies ordered into layers[6].

Raman measurements. Raman spectra were acquired exciting samples with the 632.8 nm line of a He-Ne laser and the scattered light was analyzed using a spectrometer equipped with an LN$_2$-cooled charge-coupled

device detector. The spectra were recorded in backscattering geometry in crossed and parallel polarization configurations. For the temperature dependent measurements a heating stage (THMS600 by Linkam) was employed during Raman spectra acquisition.

FIR measurements. Measurements in the far-infrared regime were carried out under vacuum conditions both in transmission and reflection geometries using a high-resolution Fourier transform infrared spectrometer (BRUKER IFS 125HR) of the THz beamline at Helmholtz-Zentrum Berlin (BESSY II)[27]. The spectral range in the presented experiments covered wavenumbers between 30 and 650 cm^{-1} (i.e., frequencies from 0.9 to 19 THz) and was limited by the selected source (internal Hg-lamp), the 6 μm multilayer-mylar beamsplitter and the detector, a 4.2 K Si-Bolometer. A copper block heating stage was employed during *in-situ* temperature dependent FIR measurements.

References

1. Raoux, S., Welnic, W. & Ielmini, D. Phase change materials and their application to nonvolatile memories. *Chem. Rev.* **110,** 240–267 (2010).
2. Yamada, N., Ohno, E., Akahira, N. & Nishiuchi, K. High Speed Overwritable Phase Change Optical Disk Material: MEDIA. *Jpn. J. Appl. Phys.* **26,** 61–66 (1987).
3. Shportko, K. *et al.* Resonant bonding in crystalline phase-change materials. *Nat. Mater.* **7,** 653–8 (2008).
4. Zhang, W. *et al.* Role of vacancies in metal-insulator transitions of crystalline phase-change materials. *Nat. Mater.* **11,** 952–6 (2012).
5. Siegrist, T. *et al.* Disorder-induced localization in crystalline phase-change materials. *Nat. Mater.* **10,** 202–208 (2011).
6. Bragaglia, V. *et al.* Metal–Insulator Transition Driven by Vacancy Ordering in GeSbTe Phase Change Materials. *Sci. Rep.* **6,** 23843 (2016).
7. Braun, W. *et al.* Epitaxy of Ge–Sb–Te phase-change memory alloys. *Appl. Phys. Lett.* **94,** 041902 (2009).
8. Först, M. *et al.* Phase change in Ge$_2$Sb$_2$Te$_5$ films investigated by coherent phonon spectroscopy. *Appl. Phys. Lett.* **77,** 1964 (2000).
9. Andrikopoulos, K. S., Yannopoulos, S. N., Kolobov, A. V., Fons, P. & Tominaga, J. Raman scattering study of GeTe and Ge$_2$Sb$_2$Te$_5$ phase-change materials. *J. Phys. Chem. Solids* **68,** 1074–1078 (2007).
10. Richter, W., Krost, A., Nowak, U. & Anastassakis, E. Anisotropy and dispersion of coupled plasmon-LO-phonon modes in Sb$_2$Te$_3$. *Zeitschrift für Krist. Phys. B Condens. Matter* **49,** 191–198 (1982).
11. Steigmeier, E. F. & Harbeke, G. Soft phonon mode and ferroelectricity in GeTe. *Solid State Commun.* **8,** 1275–1279 (1970).
12. Shu, M. J. *et al.* Ultrafast terahertz-induced response of GeSbTe phase-change materials. *Appl. Phys. Lett.* **104,** 251907 (2014).
13. Bragaglia, V. *et al.* Structural change upon annealing of amorphous GeSbTe grown on Si(111). *J. Appl. Phys.* **116,** 054913 (2014).
14. Sosso, G. C., Caravati, S., Mazzarello, R. & Bernasconi, M. Raman spectra of cubic and amorphous Ge$_2$Sb$_2$Te$_5$ from first principles. *Phys. Rev. B* **83,** 134201 (2011).
15. Nonaka, T., Ohbayashi, G., Toriumi, Y., Mori, Y. & Hashimoto, H. Crystal structure of GeTe and Ge$_2$Sb$_2$Te$_5$ meta-stable phase. *Thin Solid Films* **370,** 258–261 (2000).
16. Chen, Y. *et al.* Composition-dependent Raman modes of Mo1−xWxS2 monolayer alloys. *Nanoscale* **6,** 2833 (2014).
17. Sosso, G. C., Caravati, S., Gatti, C., Assoni, S. & Bernasconi, M. Vibrational properties of hexagonal Ge$_2$Sb$_2$Te$_5$ from first principles. *J. Phys. Condens. Matter* **21,** 245401 (2009).
18. Huang, B. & Robertson, J. Bonding origin of optical contrast in phase-change memory materials. *Phys. Rev. B* **81,** 1–4 (2010).
19. Shalini, A. *et al.* Coherent phonon modes of crystalline and amorphous Ge$_2$Sb$_2$Te$_5$ thin films: A fingerprint of structure and bonding. *J. Appl. Phys.* **117,** 025306 (2015).
20. Matsunaga, T., Kojima, R. & Yamada, N. Overview of the GeTe-Sb$_2$Te$_3$ pseudobinary crystalline phase. *epcos.org* **3,** 1–9 (2007).
21. Privitera, S., Rimini, E. & Zonca, R. Amorphous-to-crystal transition of nitrogen- and oxygen-doped Ge$_2$Sb$_2$Te$_5$ films studied by *in situ* resistance measurements. *Appl. Phys. Lett.* **85,** 3044 (2004).
22. Xu, L. *et al.* A comparative study on electrical transport properties of thin films of Ge$_1$Sb$_2$Te$_4$ and Ge$_2$Sb$_2$Te$_5$ phase-change materials. *J. Appl. Phys.* **110,** 013703 (2011).
23. Boschker, J. E. *et al.* Surface reconstruction-induced coincidence lattice formation between two-dimensionally bonded materials and a three-dimensionally bonded substrate. *Nano Lett.* **14,** 3534–8 (2014).
24. Giussani, A. *et al.* On the epitaxy of germanium telluride thin films on silicon substrates. *Phys. Status Solidi* **249,** 1939–1944 (2012).
25. Wang, R. *et al.* Toward Truly Single Crystalline GeTe Films: The Relevance of the Substrate Surface. *J. Phys. Chem. C* **118,** 29724–29730 (2014).
26. Rodenbach, P. *et al.* Epitaxial phase-change materials. *Phys. status solidi–Rapid Res. Lett.* **6,** 415–417 (2012).
27. Holldack, K. & Schnegg, A. THz Electron Paramagnetic Resonance/THz Spectroscopy at BESSY II. *J. large-scale Res. Facil. JLSRF.* **2,** A51 (2016).

Acknowledgements

Author Contributions

Samples were grown and characterized by V.B. and J.E.B. F.A. and E.Z. contributed to the interpretation of Raman spectra, T.F. performed Raman measurements. V.B. and K.H. performed FIR spectroscopy measurements. The paper was written by V.B. and R.C., with the help and through contributions from all co-authors. All authors have given approval to the final version of the manuscript. The project was initiated and conceptualized by R.C.

Additional Information

Competing financial interests: The authors declare no competing financial interests.

How to cite this article: Bragaglia, V. *et al.* Far-Infrared and Raman Spectroscopy Investigation of Phonon Modes in Amorphous and Crystalline Epitaxial GeTe-Sb$_2$Te$_3$ Alloys. *Sci. Rep.* **6,** 28560; doi: 10.1038/srep28560 (2016).